Application of Phase Change Materials for Low Duty Cycle High Peak Load Power Supplies

Andrija STUPAR, Uwe DROFENIK, and Johann W. KOLAR

Power Electronic Systems Laboratory, ETH Zurich
ETH-Zentrum / ETL H18, CH-8092 Zurich, Switzerland
Phone: +41-44-632-7447, Fax: +41-44-632-1212, E-mail: stupar@lem.ee.ethz.ch

Abstract

A power electronic device's lifetime depends on its maximum operating temperature and the temperature swings it is subjected to. Heat sinks employing phase change materials (PCMs) can be employed to achieve a temperature reduction, but only for a limited duration. This makes such heat sinks appropriate for use in applications with high peak loads but with low duty cycles. The heat sink is modelled using the thermal RC network approach, and an optimization procedure for designing a hybrid air-cooled heat sink containing PCM is developed, yielding a maximum possible temperature reduction for a given application.

1 Introduction

Power supplies having high peak loads yet low duty cycles are to be found in many up and coming applications. These are typically power electronics converters for systems which are inactive for relatively long periods of time and then need to suddenly burst into activity, such as electromechanical actuators in aircraft, namely retractors extenders for landing gear [1]. Such actuators are operated for several seconds during take-off and landing, and are then inactive for the duration of the flight, which can last several hours. Another application for which high peak low duty cycle power electronics can be used are novel ultracapacitor-powered electric buses [2], which recharge their batteries on certain stops, for 5 minutes, with 20 minutes in between charges. A generalized power profile representing applications as the above is shown in Fig. 1.

The reliability of such power converters, especially for transportation applications such as aerospace, is of great importance. Typically these power supplies are built using IGBT modules. It has been shown [3], [4] that the peak operating temperature and the temperature cycle amplitude affect the lifetime of an IGBT module. It follows that the method of cooling, that is, the thermal management of power electronic devices, is of significant importance from the reliability standpoint.

One of the usual conventional approaches to cooling power electronic devices is to place them on an air-cooled finned metal heat sink with an attached fan. An alternative are hybrid heat sinks which employ phase change materials (PCM) [6-9], as depicted in Fig. 2. In such configurations the PCM absorbs heat as it changes from solid to liquid or liquid to gas, temporarily slowing the temperature rise of the device and resulting in a lower operating temperature over a certain period. PCM heat sinks are well suited for high peak load low duty cycle applications: the PCM absorbs the heat, lowering the device temperature, and then follows a long period of inactivity during which this absorbed heat can be released to the ambient. However, there are tradeoffs involved with this approach: while adding PCM increases the peak thermal capacity of the heat sink, it also significantly increases its thermal resistance.

This paper presents an optimization procedure for designing a hybrid PCM-metal heat sink so as to arrive at a maximum reduction of the peak operating temperature compared to a conventional heat sink of equivalent volume. To achieve this, a thermal network model is developed, allowing for quick simulations and comparisons of different designs.

Section 2 of this paper briefly explains previous heat sink optimization work that it builds on. Section 3 discusses

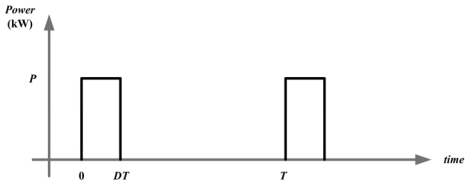

Figure 1 – A generalized high peak load low duty cycle power profile, with peak power *P* and period *T* much greater than on time *DT*.

how the PCM is modelled, different possible configurations of the heat sink as well as material properties, and presents the optimization procedure, while Section 4 gives

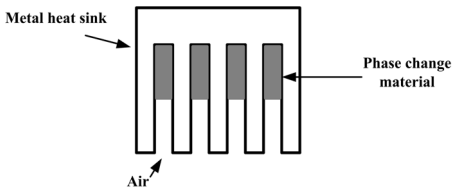

Figure 2 – A hybrid heat sink, with a portion of the channels filled with phase change material (gray), and the rest free for air flow.

ISBN 978-3-8007-3212-8

its result for a particular example. In that section also the results given by the thermal network model are compared to results from 3D-FEM simulations. Section 5 extends the model to a PCM-metal matrix. Section 6 considers future work and conclusions are given in Section 7.

2 Optimizing Air-Cooled Heat sinks

This paper builds on previous work [10-11] done for optimizing fan-cooled heat sinks. The optimization procedure for air-cooled heat sinks uses analytical and empirical equations expressions for the air flow through the heat sink and the resulting thermal resistance of the heat sink, which is then minimized by varying the heat sink fin dimensions. The relevant parameters are shown in Fig. 3. A detailed discussion of the mathematical procedure and the equations (1) – (14), and the accuracy of the theory verified by experimental results, can be found in [10], [12]. This procedure and by extension this paper is limited to the commonly found heat sink shape shown in Fig. 3.

k	fin spacing ratio
λ_{HS} (W/mK)	thermal conductivity of heat sink material
A_{HS} (m^2)	size of the heat sink base plate
d_h (m)	hydraulic diameter of one channel
L (m)	channel length in air flow direction
n	number of channels
Δp (N/m^2)	pressure drop in one channel
V (m^3/s)	volume flow
Re_m	avg. Reynolds number (for lam. or turb. flow)
Nu_m	avg. Nusselt number (for lam. or turb. flow)
h (W/m^{2}K)	(convective) heat transfer coefficient
$Pr \approx 0.71$	Prandtl number (air, 80°C)
$\rho_{AIR} \approx 0.99$ (kg/m^3)	air density (80°C)
$\nu_{AIR} \approx 2.1$e-5 (m^2/s)	cinematic viscosity of the air (80°C)
$c_{p,AIR} \approx 1010$ (J/kgK)	specific thermal capacitance of air
$\lambda_{AIR} \approx 0.03$ (W/mK)	thermal conductivity of air (80°C)

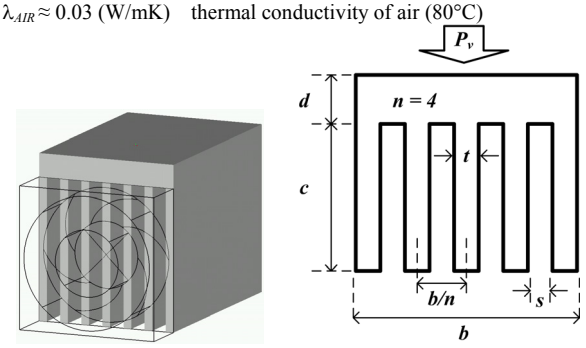

Figure 3 – The air-cooled heat sink shape considered for optimization, with dimensions shown.

$$k = \frac{s}{b/n} \tag{1}$$

$$d_h = \frac{2s \cdot c}{s + c} \tag{2}$$

$$\Delta p_{lam}(V) = \frac{48\, \rho_{AIR}\, \nu_{AIR}\, L}{n\,(s \cdot c)\, d_h^2}\ V \tag{3}$$

$$\Delta p_{turb}(V) = \frac{L \frac{s+c}{2s \cdot c}\, \rho_{AIR}\, \frac{1}{2} (\frac{V}{n(s \cdot c)})^2}{(0.79 \cdot \ln(\frac{2V}{n\,(s+c)\nu_{AIR}}) - 1.64)^2} \tag{4}$$

$$Re_m = \frac{2V}{n(s+c)\nu_{AIR}} \tag{5}$$

$$k \cdot \Delta p_{FAN}\,(V) = \Delta p_{lam}(V_{lam}) \ \rightarrow V_{lam} \ \text{ if } (Re_{m,lam} < 2300) \tag{6}$$

$$Nu_{m,lam} = \frac{3.657 \left[\tanh\left(2.264 X^{1/3} + 1.7 X^{2/3}\right)\right]^{-1} + \frac{0.0499}{X} \tanh(X)}{\tanh\left[2.432\ Pr^{1/6} X^{1/6}\right]} \tag{7}$$

$$X = \frac{L}{d_h\, Re_m\, Pr} \tag{8}$$

$$Nu_{m,turb} = \frac{\{8 \cdot (0.79 \cdot \ln(Re_m) - 1.64)^2)\}^{-1} (Re_m - 1000)\ Pr}{1 + 12.7 \sqrt{\{8 \cdot (0.79 \cdot \ln(Re_m) - 1.64)^2)\}^{-1}}\ (Pr^{2/3} - 1)} \cdot \left(1 + \left(\frac{d_h}{L}\right)^{2/3}\right) \tag{9}$$

The optimization procedure begins with the selection of fan, which then defines the heat sink dimensions b x c. The flow of air through the channels can be laminar or turbulent, with the pressure drop along the channel defined by (3) and (4), respectively. The air flow through the channels is found where (3) (for laminar flow) or (4) (turbulent) intersects with the pressure-flow fan characteristic obtainable from the fan datasheet. This is used to calculate the Reynolds number and (5) and (6) is used to determine whether the flow is laminar or turbulent – a Reynolds number less than 2300 indicates laminar flow. Knowing this the appropriate Nusselt number can be calculated using (7) or (9). This allows then for the calculation of the heat transfer coefficient h (10). The transfer of heat from the heat sink surface to the air in one channel can be represented as a network of thermal resistors and capacitors, shown in Fig. 4.

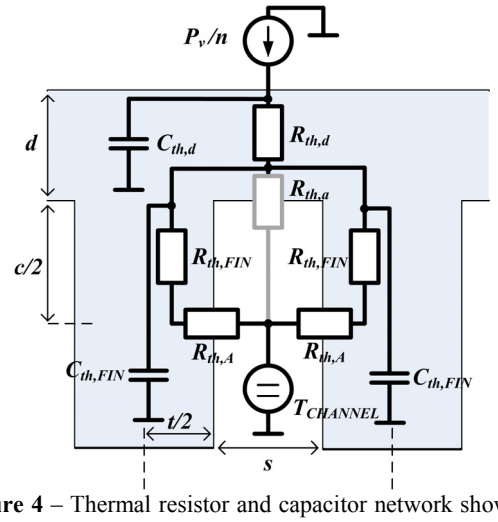

Figure 4 – Thermal resistor and capacitor network showing the heat flow through one channel of the heat sink.

For the optimization procedure, the capacitors are ignored. For geometries with $s << c$, $R_{th,a}$ is much greater than $R_{th,A}$ and can be ignored [10]. The rest of the resistances can be calculated using (10) – (13).

$$h = \frac{Nu_m \cdot \lambda_{AIR}}{d_h} \tag{10}$$

$$R_{th,A} = \frac{1}{h \cdot L \cdot c} \tag{11}$$

ISBN 978-3-8007-3212-8

$$R_{th,FIN} = \frac{\frac{1}{2}c}{\frac{1}{2}t \cdot L \cdot \lambda_{HS}} \quad (12)$$

$$R_{th,d} = \frac{d}{\frac{1}{n}A_{HS}\lambda_{HS}} \quad (13)$$

$$R_{th,S-a}^{(HS)} = \frac{1}{n}(R_{th,d} + \frac{1}{2}(R_{th,FIN} + R_{th,A})) + \frac{0.5}{\rho_{AIR}\, c_{P,AIR}\, V} \quad (14)$$

Eqn. (14) gives the total thermal resistance of the heat sink. The term on the right represents the average temperature rise of the air in the channel due to the heat transported away by convection. The optimization procedure therefore consists of varying the dimensions *s* and *t* (or one of those and the number of channels *n*), for a given fan, until the minimum total thermal resistance, calculated using (1) – (14), is found.

3 Optimizing Hybrid PCM Heat Sinks

To arrive at an optimization procedure for a hybrid heat sink which is both air-cooled and contains phase change material, the method of Section 2 is extended to include the effects of the PCM. Therefore, a corresponding thermal network must be found. To start, first the properties of the material are considered.

3.1 Phase-change material properties

The properties of some phase-change materials commonly cited in literature [5-7], [9], [13-14] are given in Table 1. In [5-7], [9] PCMs which change phase from solid to liquid are investigated, in [13] pentaglycerine (PG) undergoing a solid-solid phase transition is examined, while [14] deals with paraffin-water emulsions. Aluminium is chosen as the material for the metal part of the heat sink; its properties are also given in Table 1.

The first parameter which is examined is the melting (i.e. phase change) temperature T_{melt}. Obviously the melting temperature should be above the ambient temperature; the change of phase is the heat absorption mechanism, and this should happen only after a power pulse is applied. The ambient temperature for this paper is selected as 45°C (a typical industrial setting). This therefore removes from this investigation any PCMs with a lower T_{melt}, i.e. the first three materials in the table, and the paraffin-water emulsions of [14], which have T_{melt} in the range 0-20°C. Furthermore it is advantageous to have the T_{melt} close to the ambient temperature, so that the phase change beings as soon as the power pulse is applied, so that heat is absorbed right away. Next, perhaps the parameter of most interest is the latent heat of melting ΔH, which specifies the heat absorbed during the change of phase. Of interest are also the density ρ and specific heat capacity C_p. Among the materials in Table 1 therefore, Suntech P116, which is a type of paraffin wax, is selected as it has a melting temperature close to but above the ambient, the highest latent heat, and a greater heat capacity-density product (i.e. heat capacity per volume) than the metallic alloy PCM or PG. Also note the low thermal conductivity λ of all the PCMs.

Table 1 – The thermal properties of phase change materials and aluminium.

Material	ρ kg/m^3	λ W/mK	ΔH kJ/kg	T_{melt} °C	C_p J/kgK
Octadecane	774	0.35	244	28	-
Eicosane	785	0.15	247	36	2460
Heneicosane	788	0.15	213	40	-
Suntech P116	818	0.24	266	47	2730
Metallic alloy [6]	9160	15.0	14	47	147
PG (solid-solid)	750	0.17	177	83	2350
Aluminium	2700	210	-	-	903

3.2 Modelling the phase-change material

Mathematical models of phase-change materials are well-established and experimentally verified [7-9], [13-15]. Adopted here is the variable specific heat capacity approach of [9], [13], [15]. Essentially, the specific heat capacity of the PCM increases by $\Delta H/\Delta T$, where ΔT is the temperature range over which the PCM melts. In [9] it is shown that a realistic range is $\Delta T = 3$°C. Therefore the apparent heat capacity [9] of the PCM, C_{app}, can be defined as:

$$C_{app} = \begin{cases} C_p & \text{for } T \le T_{melt} \\ C_p + \Delta H/\Delta T & \text{for } T_{melt} < T < T_{melt} + \Delta T \\ C_p & \text{for } T \ge T_{melt} \end{cases} \quad (15)$$

As in [6-7], to simplify the modelling, all the other material properties are assumed constant over the entire temperature range under consideration. The effect of the molten material flowing can also be ignored [6-7]. Using the material properties, a thermal network model of a single PCM block is developed, shown in Fig. 5. A rectangular volume of PCM is divided into four equivalent thermal resistors (conduction from all sides) with a single thermal capacitor for the entire volume placed in the midpoint. Eqns. (16) – (18) give the definitions for the elements of the thermal circuit in Fig. 5. The dimensions h_{PCM}, w_{PCM} and l_{PCM} are the height, width, and length of the PCM

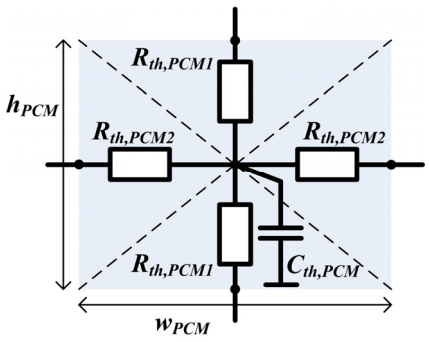

Figure 5 – Thermal resistor and capacitor network model of rectangular volume of phase change material.

ISBN 978-3-8007-3212-8

block, respectively and λ_{PCM} and ρ_{PCM} are the thermal conductivity and density of the material, respectively.

$$R_{th,PCM1} = \frac{\frac{1}{2} h_{PCM}}{\frac{1}{2} w_{PCM} l_{PCM} \lambda_{PCM}} \quad (16)$$

$$R_{th,PCM2} = \frac{\frac{1}{2} w_{PCM}}{\frac{1}{2} w_{PCM} l_{PCM} \lambda_{PCM}} \quad (17)$$

$$C_{th,PCM} = h_{PCM} w_{PCM} l_{PCM} \rho_{PCM} C_{app} \quad (18)$$

3.3 Different PCM heat sink configurations

Different heat sink configurations are found in literature [5-9], [13-16]. The most common approaches are shown in Fig. 6. In [5], [13], [17], and [18] optimization techniques for the configuration of Fig. 6(b) are presented. In this configuration there is no airflow between the fins, and the procedure of Section 2 therefore cannot be applied; also, this configuration is characterised by a large thermal resistance due to the PCM's low conductivity, and a very slow ejection of heat to the ambient once the power pulse has passed, since there is no fan and associated forced air flow. For these reasons the configuration of Fig. 6(b) is not considered further in this paper. The configuration of Fig. 6(c) is the topic of [16], where the PCM is embedded in the heat sink fins. The optimization procedure of Section 2 tends to produce fin thicknesses in the order of a few millimetres. With that in mind, the configuration of Fig. 6(c) would be very difficult (if not impossible) to manufacture, and it is therefore not considered further. This leaves configurations Fig. 6(a) [7], where the tips of the fins are immersed in PCM, and Fig. 6(d) [6], where

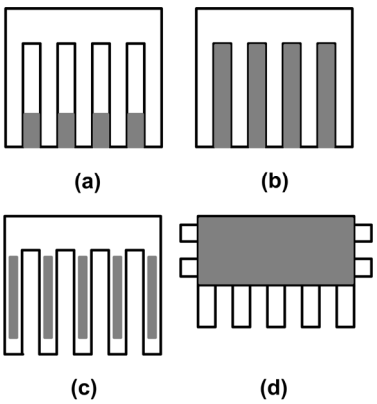

Figure 6 – Different combinations of PCM heat sinks found in literature; phase change material shown in gray.

the heat source is placed on top of a large PCM-filled compartment. The advantage of the latter is the PCM is close to the heat source, allowing for quick heat absorption. The disadvantage is that the thermal resistance of such a heat sink from heat source to the ambient air is very high, due to the low thermal conductivity of the PCM, meaning that the heat sink performance degrades greatly as compared to a regular heat sink once the PCM is melted. The advantage of the former is that a large section of the heat sink can be left open for air flow, with a thermal resistance from heat source to the air comparable to that of a conventional heat sink. The disadvantage is that the PCM is farther from the heat source, and so it takes longer for the heat to reach it.

3.3.1 Selected heat sink configuration

An obvious approach is then to somehow combine the advantages of the configurations of Fig. 6(a) and Fig. 6(d). Analyzing from the perspective of the thermal networks in Figs. 4 and 5, and keeping in mind the properties of the materials, the following design guidelines become clear:

- Since $\lambda_{PCM} << \lambda_{HS}$, we have $R_{th,PCM1} >> R_{th,d}$, and therefore there should be a path of metal from the heat source to the fins; in this way, once the PCM is melted, heat can flow from the heat source to the ambient effectively bypassing the high-resistance PCM.
- The results of optimizations of PCM-metal heat sinks from [5], [13], [17-18] show that the PCM should not be one monolithic block, but divided into several cells surrounded by metal, as to improve the heat transfer into and out of the material.
- The $C_p \cdot \rho$ product, i.e. the heat capacity per volume, is greater for aluminium than for the chosen PCM, meaning that outside of the phase transition, the PCM will have a lower thermal capacitance than an equivalent volume of the metal. This suggest that replacing air with PCM is preferable to replacing metal with PCM, as the former increases resistance but also capacitance, while the latter increases resistance and decreases the capacitance (outside of the phase transition). Furthermore, as discussed in [10], decreasing base plate thickness d decreases the heat spreading effect of the base plate, which is undesirable.
- The thermal resistance between the heat source and the PCM should be minimized.

Following these guidelines, the resulting heat sink configuration is one where the base plate is unmodified and the PCM is placed between the fins, but moved closer to the heat source – it is placed at the beginning of the fins, right after the base plate, rather than at the fins. This is the configuration shown in Fig. 1, and also in more detail in Fig. 7(a).

3.3.2 PCM Heat sink thermal network

The thermal network for one channel of the selected heat sink configuration is given in Fig. 7(b). Eqns. (19) – (24) give the expressions for the elements of the network. Terms not defined here are the same as in Section 2. The resistor from the PCM to the ambient is ignored for the same reason as $R_{th,a}$ in Section 2.

$$R_{th,FIN-PCM} = \frac{\frac{1}{2} c_{PCM}}{\frac{1}{2} t \cdot L \cdot \lambda_{HS}} \quad (19)$$

$$C_{th,d} = \frac{1}{n} A_{HS} \rho_{HS} C_{HS} \quad (20)$$

$$C_{th,d} = \frac{1}{2} tLs \rho_{HS} C_{HS} \quad (21)$$

$$R_{th,PCM1} = \frac{\frac{1}{2} c_{PCM}}{\frac{1}{2} sL\lambda_{PCM}} \quad (22)$$

ISBN 978-3-8007-3212-8

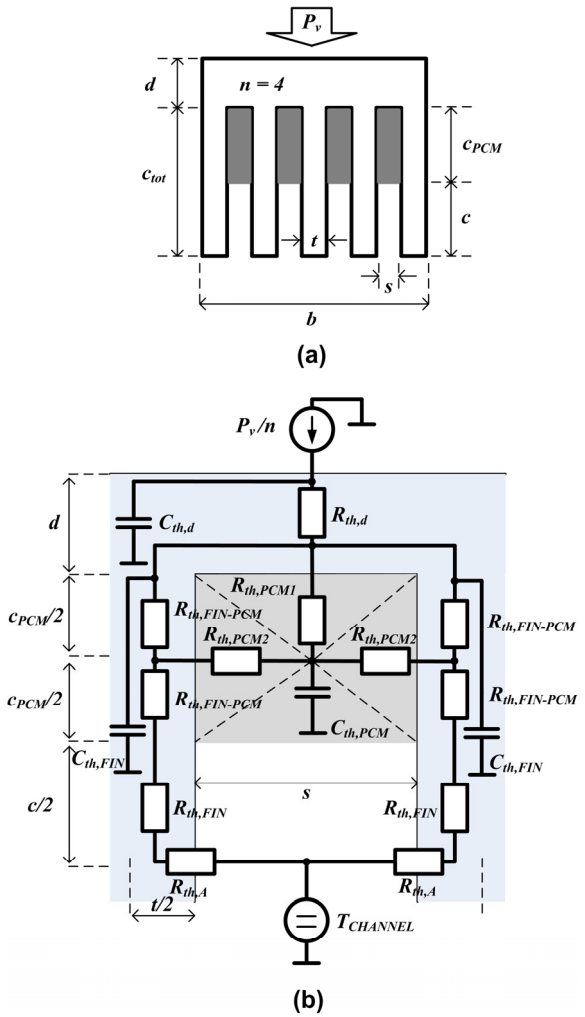

Figure 7 – (a) chosen hybrid PCM heat sink configuration with dimensions shown (b) Thermal resistance and capacitance network showing the heat flow through one channel of the PCM heat sink

$$R_{th,PCM2} = \frac{\frac{1}{2}s}{\frac{1}{2}c_{PCM}L\lambda_{PCM}} \tag{23}$$

$$C_{th,PCM} = sc_{PCM}L\rho_{PCM}C_{app} \tag{24}$$

The dimension c is the height of the channel exposed to air flow, while c_{PCM} is the height of the channel filled with PCM, and ρ_{HS} and C_{HS} are the density and specific heat capacity of the metal.

3.4 Optimization Procedure

Due to the tradeoffs involved with adding PCM to a heat sink, it is not simply enough to optimize for a final stationary thermal resistance as in Section 2. Adding PCM increases thermal resistance, but also adds a large variable capacitance. Whether a particular PCM heat sink is useful for a pulsed-power application therefore depends on the transient properties of the heat sink and the characteristics of the power pulse – its amplitude and duration. Therefore, to compare heat sink with varying amounts of PCM, simulations of the response of heat sink thermal RC network to the pulse must be performed. In this way different variations can be compared and the optimum dimensions chosen. The optimization procedure of Section 2 can be performed on a computer in seconds. The simulation of a derived thermal RC network can also be performed in seconds with the help of a circuit simulator. If that is compared to the significantly longer simulation times needed to simulate heat sink structures in 3D finite element method (3D-FEM) simulators, the advantage of the thermal RC model approach becomes apparent.

The optimization procedure can be then broadly described by the following steps:

1. *Pick a set of heat sink dimensions.*
2. *Use the equations of Section 2 and 3.2.2 to derive the thermal network of the heat sink.*
3. *Obtain the response of the network to the desired power pulse.*
4. *Repeat steps 1 – 3 until all variations are exhausted.*
5. *Compare responses and pick the heat sink with the greatest temperature reduction.*

The following sub-sections explain the optimization procedure in more detail.

3.4.1 Full optimization

The method of Section 2 varies the heat sink fin thickness and the number of channels until the minimum thermal resistance is achieved with a given fan (and thus air flow). With the heat sink where PCM is added in between the fins, the varying of these parameters also affects the volume of PCM added to the heat sink. A complete optimization procedure would then vary the parameters c_{PCM}, t and n, and compare the response of each variation until and optimum is found. However, this would require simulating and comparing a very large number of possible geometries; for this reason, this approach is not undertaken in this paper. Moreover, as noted in [10], the optimization procedure of Section 2 tends to produce thin fins and generally $s > t$, so often the theoretical optimum is very difficult or impossible to manufacture. For this reason the assumption is made that the PCM cell width s is near the optimum of what is physically producible for any channel width s given as optimal by the procedure in Section 2.

3.4.2 Partial optimization

The approach taken in this paper therefore is to optimize the parameters n, s, and t for a given area b x c. First, b x c is defined by the chosen fan and c_{PCM} is set to zero to obtain an optimized conventional heat sink. Then c_{PCM} is incremented by an amount, and correspondingly c is decremented by the same amount. The new optimal set of parameters n, s, and t is then found for the new area b x c, using the method of Section 2. The procedure is repeated until the channels are fully filled with PCM (this last variation is discarded as there is no air flow). At each step the thermal network is calculated; the responses of the networks are then compared to obtain the optimum dimensions.

Note that each time PCM is added, the available area for air flow decreases. The assumption made during this op-

ISBN 978-3-8007-3212-8

timization procedure is that the fan however remains fully utilized; i.e. all the air which would be forced through the conventional heat sink area b x c_{tot} is forced through the reduced areas b x c for each variation of the PCM amount. Instead of the portion of the fan facing the PCM simply being blocked, an air guide or duct can be constructed to direct all the air into the reduced area. It is assumed that if this duct is constructed with a mild slope (no abrupt bends) and of a low resistance material (i.e. a smooth plastic) then no significant pressure loss compared to the heat sink without PCM occurs.

3.4.3 Optimizing the amount of added PCM

A simpler approach that may be of practical interest is to simply add PCM to the conventional heat sink, i.e. vary c_{PCM} but without re-optimizing the remaining parameters at each step. This may be useful in a situation where for example the power system designer wishes to improve the performance of a commercially available heat sink by adding PCM, which can be purchased separately.

4 Optimization Example

A particular optimization scenario, with results is presented in this section. Also, the results obtained are compared with a 3D-FEM simulation of the PCM heat sink performed using the *IcePak* software.

4.1 Power profile

As the optimization procedure is application-specific, high peak power low duty cycle applications such as those mentioned in Section 1 were examined. Power electronic devices that are suitable for such applications and their losses dissipated to the heat sink as heat were investigated. The heat sink dimensions L x b were chosen as to have the power electronics module cover the entire area of the heat sink. A loss per area of the heat sink figure of 5 W/cm^2 was found to be an adequate representation of a range of applications and appropriate modules.

Table 2 – Conventional heat sink (optimized without PCM) dimensions (mm).

b	c	L	n	s	t
60	60	110	18	2.3	1.0

4.2 Conventional heat sink without PCM

The dimensions L = 110 mm and b = 60 mm were chosen, giving a heat sink area that can accommodate several kinds of commercial IGBT modules. An according fan with dimensions b = c = 60 mm was then chosen, in this case the Sanyo Denki *9WP0612H402* [19]. The minimum fin thickness was set at t = 1.0 mm, to reflect a heat sink that can realistically be manufactured. Using the procedure of Section 2, the optimized conventional heat sink was found with n = 18, s = 2.3 mm and t = 1.0 mm.
Using the previous figure for losses of 5 W/cm^2, the heat sink area gives a power pulse with an amplitude of 330 W. The heat sink dimensions are summarized in Table 2.

4.3 Optimized heat sink dimensions with PCM included

The method of Section 3.4.2 was applied: in this case c_{PCM} was first incremented by 5 mm from 0 to 55 mm. The diminishing available area for air flow was then re-optimized at each step. As c_{PCM} was increased, the optimization routine gave smaller and smaller fin thickness t, decreasing to below 1.0 mm. When the thickness was limited to a manufacturable 1.0 mm as in the previous section, at each step the optimization yielded either the same dimensions as the conventional heat sink, or a very similar configuration of n = 19, s = 2.1 mm, t = 1.0 mm. For this reason the simpler method of Section 3.4.3 was used for the next steps: only the amount of PCM was varied while the other dimensions were kept the same as in Table 2.

4.4 Comparison with 3D-FEM simulations

In the absence of experimental results, the output of the thermal network model was compared to 3D simulations of the hybrid PCM heat sink. As in [10], there is a difference of approximately 20% compared to the results using the thermal network. Also as in [10], the overall thermal resistance calculated by the thermal model is greater than that obtained through 3D-FEM simulation. An error is to be expected since the many hundreds or thousands of simulated cells of a 3D simulation are reduced by the thermal network model to only a few cells, and because of the many approximations of the analytical expressions (see [10]). It should be noted also that in [10], where the method of Section 2 is derived and verified experimentally, the experimental measurements yielded values in between, less than those given by the thermal network model but greater than derived from the 3D simulation. Experiments will be performed in the future for further verification of the model.
Although there is a difference between the absolute numerical values of the two simulations, the general behaviour of the curves is the same. The step responses of the conventional heat sink and a heat sink with one third of the channel height filled with PCM (c_{PCM} = 20 mm) to a 330 W step from both the thermal network model and 3D model are given in Fig. 8.
In order to quantify the transient performance of the PCM heat sink for comparison between the two simulations, the area under (i.e. the integral of) the step-response curve for the conventional heat sink $\int T(t)dt$ is considered. The area in between the two curves, the curve for the conventional heat sink with no PCM and for the heat sink with PCM, $\int \Delta T(t)dt$, can then be thought of as a reduction of the original area $\int T(t)dt$, allowing for the definition of a relative improvement index Q_I:

$$Q_I = \frac{\int_0^{t_{int}} \Delta T(t)dt}{\int_0^{t_{int}} T(t)dt} \qquad (25)$$

The absolute temperature reduction ΔT at a given time of the PCM heat sink compared to the conventional heat sink is also compared. These values are summarized in Table 3. Again, the values differ by approximately 20%. Com-

ISBN 978-3-8007-3212-8

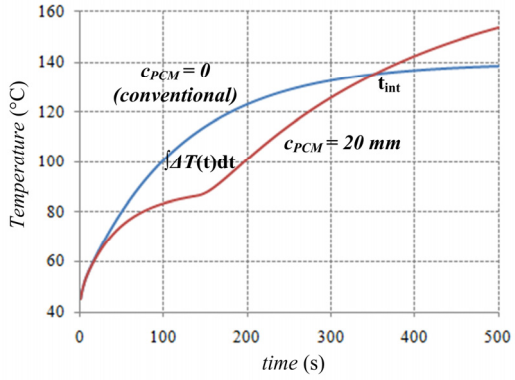

(a) Thermal network simulation

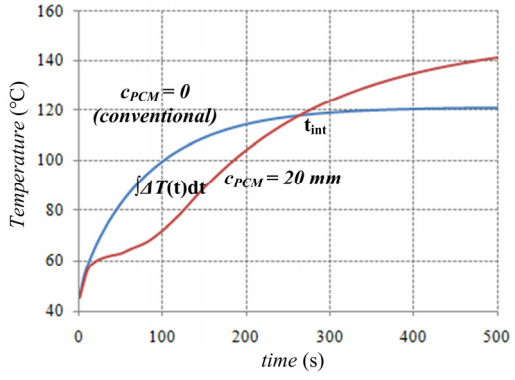

(b) 3D-FEM simulation

Figure 8 – Response to a 330 W step, heat sinks with no PCM and with a third of the channel length filled with PCM; a) thermal RC network simulation, b) IcePak simulation.

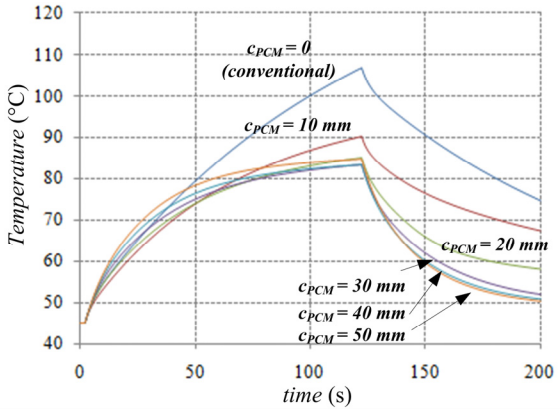

Figure 9 – Response to a 330 W pulse of duration 120 s of heat sinks with varying amounts of PCM.

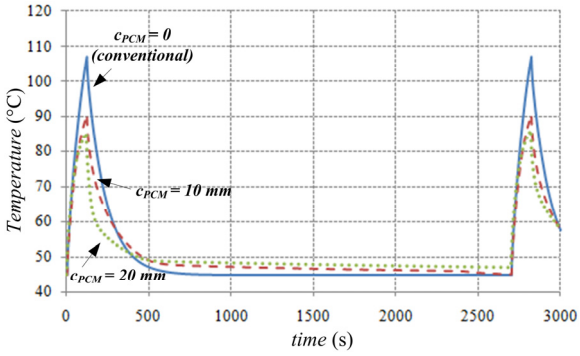

Figure 10 – The response to two consecutive pulses of the conventional heat sink (solid line), c_{PCM} = 10 mm (dashed), and c_{PCM} = 20 mm (dotted).

pared to the 3D-FEM simulations, it can be said the thermal network model underestimates the improvement gained by adding PCM. It is clear the thermal network modelling approach is a good guideline for optimizing hybrid PCM heat sinks.

Table 3 – Comparison of the relative improvement gained by adding PCM to a heat sink from two different simulations.

	Thermal network	3D-FEM
$R_{th,S-a}^{(HS)}$, c_{PCM} = 0 (K/W)	0.29	0.23
Q_1	0.117	0.152
Temp. (°C) at t = 120 s, c_{PCM} = 0	107	104.2
Temp. (°C) at t = 120 s, c_{PCM} = 20 mm	85.7	78.4
ΔT at t = 120 s	21.3	25.8
Temp. reduction compared to c_{PCM} = 0 (%)	19.9	24.8

4.5 Optimization results

Adding PCM to the heat sink increases its thermal resistance; that is why once the PCM is melted, the temperature of the PCM heat sink surfaces exceeds that of the conventional heat sink, assuming a constant power input, as can be seen in Fig. 8. Therefore there is a certain range, or power pulse width, over which the PCM heat sink is useful. The re-solidification of the PCM during which it ejects the heat to ambient must also be taken into consideration; if the PCM does not re-solidify by the time the next power pulse arrives, the advantages of the phase change heat absorption mechanism will not be utilized. Therefore a specific load period and duty cycle must be selected. Note from Fig. 8 the slow response (tens to hundreds of seconds) of the PCM: the hybrid heat sink confers no advantage to situations where the pulse is only several seconds long or shorter. To complete the procedure consider for example the application of an ultracapacitor powered road vehicle (similar to [2]) which can recharge its capacitors in 2 minutes and go 45 minutes between charges. The response to the corresponding pulse of 330 W, period 2700 seconds, duty ratio 0.044 (120 seconds) is given in Fig. 9. Fig. 9 shows the first 200 s of the period, with the peak temperature for configurations with $0 \leq c_{PCM} \leq 50$ mm, varied at 10 mm increments. As PCM is added, the peak temperature is reduced. From this it might seem that the configuration with the most PCM should be selected; however, the re-solidification phase must also be examined. Also, it is not clear how well the fan assumption of Section 3.4.2 holds with the available area for air flow reduced by more than two-thirds.

ISBN 978-3-8007-3212-8

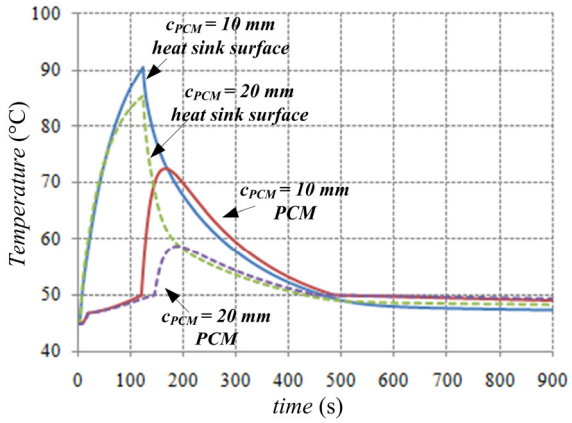

Figure 11 – The temperature of the heat sink surface and of the PCM itself during the pulse for c_{PCM} = 10 mm (solid line) and c_{PCM} = 20 mm (dashed). Note the larger difference between the two temperatures when there is more PCM.

Table 4 – Performance of different heat sink configurations with varying amounts of PCM: the first pulse at 120 s, the end of period at 2700 s, and the second pulse at 2820 s.

	Temperature (°C)		
PCM (mm)	t = 120 s	t = 2700 s	t = 2820 s
c_{PCM} = 0	106.3	45.0	106.3
c_{PCM} = 10	90.1	45.2	90.1
c_{PCM} = 20	85.1	47.0	85.7
c_{PCM} = 30	83.3	47.7	84.6
c_{PCM} = 40	83.4	48.0	84.7
c_{PCM} = 50	84.7	48.3	86.3

Note that from Fig. 9 it would appear that the heat sinks with more PCM cool more quickly. As seen in Fig. 10 however, which shows two pulses, this is only a temporary effect, which can be explained by examining Fig. 11, showing the temperature of the heat sink surface as well as of the PCM. The more PCM is added, the higher the capacity of the PCM, the higher the thermal resistance between the PCM and the metal, and therefore the higher the temperature difference between the heat sink surface and the PCM. Hence the initial decoupling: the metal, being hotter, first cools down to the temperature of the PCM, and then the two continue to cool at a slower rate. Eventually the heat sinks with less PCM settle down to a lower temperature than those with more. The same behaviour is seen in 3D simulations.

Table 4 summarizes the performance of the configurations; as can be seen, only the configuration with c_{PCM} = 10 mm re-solidifies in time for the next pulse, while all the others are still partly molten at that point, and so their peak temperatures during the second pulse are higher than in the first. Therefore the configuration c_{PCM} = 10 mm is selected as the optimum heat sink for this application. Compared to the conventional heat sink, the peak temperature is reduced by 16°C.

5 Extending the Model to a PCM-Metal Matrix

One way to mitigate the low thermal conductivity of PCM is to embed it in a matrix of high conductivity material, as done in [15] with PCM-filled carbon foam. One element of such a matrix, or foam, can then be modelled as a cube of metal (high conductivity) inside of which there is another cube of PCM (low conductivity), as shown in Fig. 12. Eqns. (26) – (30) give the expressions for the thermal circuit elements. Using standard network transformations, the thermal network of Fig. 12 can be reduced to the network of Fig. 13, with the corresponding equivalent resistors defined by (31) and (32). The network for n cubes connected in parallel in a plane is given in Fig. 14(a). To model a three-dimensional structure of such cubes, several plane networks are connected in the manner of Fig. 14(b).

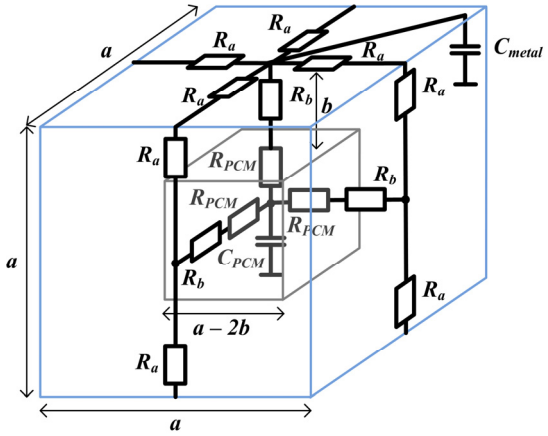

Figure 12 – Model of an element of a PCM-metal matrix: outer cube of metal, inner cube of PCM. The bottom face contains the same circuit as the top, and all the side faces the same as on the two sides shown. Heat is applied only from the top, therefore there is no horizontal conduction on the side faces. Since heat is uniformly distributed from the top, there is also no horizontal conduction from to cube to cube in a plane, only vertically from one plane to another.

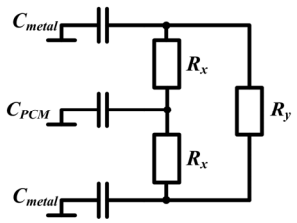

Figure 13 – Simplified model of the cell of Fig. 13 obtainable via circuit network transformations.

$$R_a = \frac{a}{\lambda_{metal} \cdot b} \tag{26}$$

$$R_b = \frac{b}{\lambda_{metal}(a-b)^2} \tag{27}$$

$$R_{PCM} = \frac{1}{\lambda_{PC} \cdot (a/2-b)} \tag{28}$$

$$C_{metal} = \tfrac{1}{2}[a^3 - (a-2b)^3]\rho_{metal}C_{Pmetal} \quad (29)$$

$$C_{PCM} = (a-2b)^3 \rho_{PC}C_{PPC} \quad (30)$$

$$R_x = \left(\frac{1}{R_b + R_{PC}} + \frac{2}{R_a + R_b + R_{PC}}\right)^{-1} \quad (31)$$

$$R_y = R_a \cdot \left(1 + \frac{R_a}{R_b + R_{PC}}\right) \quad (32)$$

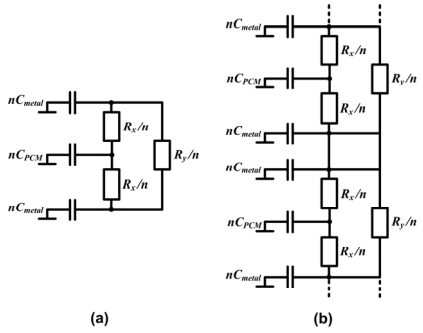

Figure 14 – (a) Model of *n* cells of Fig. 12 connected in a plane in parallel; (b) Model of a three dimensional stack of cells.

To examine the effects of the PCM-metal matrix structure, the heat sink configuration of Fig. 15 is considered, where the solid metal base plate of the conventional heat sink of Section 4 is replaced by the PCM-metal foam structure. The fins are left completely free for air flow.

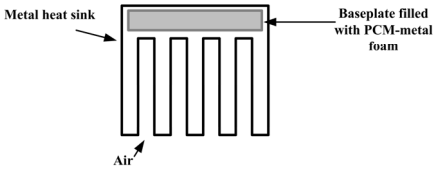

Figure 15 – Heat sink with PCM-metal matrix structure (foam) embedded in the base plate.

The base plate therefore consists of several shown in Fig. 12. The cell size is varied, giving a varying number of cells for the 10 mm x 60 mm x 110 mm base plate. The initial configuration is that of cubes with side length 10 mm, giving 66 cells for the entire base plate. The smallest cube side length examined is 250 µm, a realistic lower limit [15], yielding a matrix of 105600 cells for the entire base plate. Note that the total volume of PCM and metal respectively remains constant. The first 80 s of the response of the different matrix configurations to a 330 W step is given in Fig. 16. Here the volume of each cell is 50% PCM and 50% metal. The first conclusion that can be drawn from this graph is that embedding PCM in the base plate is not a good approach, as the temperature reduction is at most 2-4°C. However, a second more general conclusion can be drawn regarding the matrix structure itself. The more cells in the matrix, the sooner the PCM begins to melt, and the sooner the temperature-reducing effect of PCM is seen. This is because a finer matrix structure provides more high conductivity paths via the metal and heat can reach more of the PCM more quickly. This means that, as seen in Fig. 16, that the finer matrices

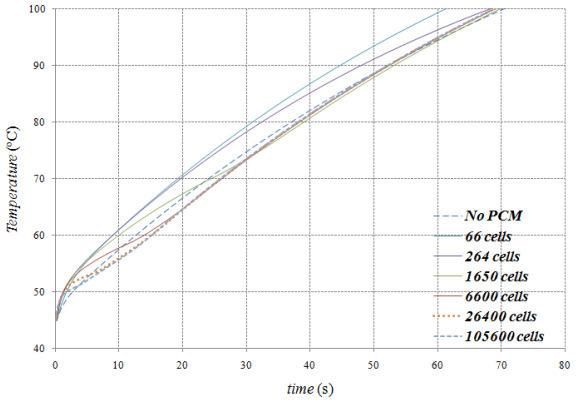

Figure 16 – Response of different PCM-metal matrix combinations, all 50% PCM 50% metal, to a 330 W step. All of the variations with PCM eventually converge to the same value.

are initially, for a short period of a few seconds or fractions of a second, hotter than configurations with fewer cells or with no PCM at all. This can also be explained by the fact that the apparent capacitance of the metal is smaller in the finer structures with more cells, since it is more distributed and divided up between cells, with more thermal resistance in between. However since the PCM heats up faster, the effect of the phase change is seen earlier, and so the finer matrices with more cells produce ultimately a larger temperature reduction, and earlier, than those with less. As can be seen in Fig. 11, with the uniform PCM structure used in Section 4, the PCM begins to melt at around 20 s after the pulse is applied. Looking at Fig. 16 however, with a fine structured PCM-metal foam consisting of tens of thousands of cells, the melting be-

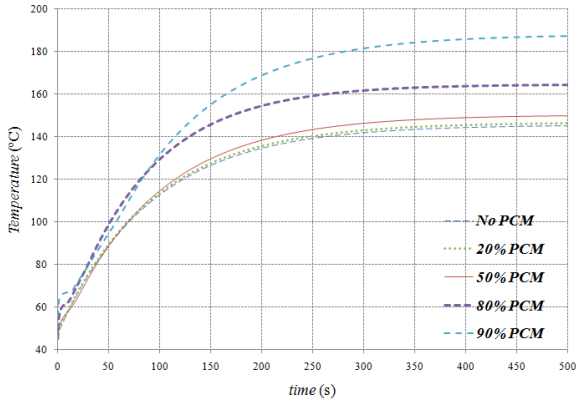

Figure 17 – Response of a 6600 cell PCM-foam matrix with varying amounts of PCM to a 330 W step.

gins 2-5 s after the pulse is applied. This suggest that the foam structure can make hybrid PCM heat sinks useful for applications with pulse lengths of seconds and tens of seconds, rather than minutes as in Section 4, for example the aerospace actuators in [1].

Finally the amount of PCM within the matrix was also varied. Fig. 17 shows the response to a 330 W of a matrix of 6600 cells with varying amounts of PCM. Above 50% of PCM, the PCM matrix actually performs worse than the conventional heat sink. This is because replacing metal with PCM increases the thermal resistance, and also

ISBN 978-3-8007-3212-8

decreases the thermal capacitance prior to melting since the heat capacity per unit volume of the PCM before it melts is actually slightly lower than that of the metal (see Section 3.3.1).

6 Future Work

The most important future task is to verify experimentally the model and procedure presented in this paper by building heat sinks with PCM added. Another area of investigation is to see what kind of potential for volume reduction hybrid PCM heat sinks offer, i.e. whether it is possible to construct a hybrid PCM heat sink of equivalent performance as a conventional one, but of smaller volume. Further investigation of the PCM-metal foam concept is required, for example the examination of the performance of configurations where such foam is placed in between the fins rather than in the base plate.

7 Conclusions

Hybrid heat sinks which are partially air-cooled and partially filled with phase change materials offer a way to reduce the peak temperature amplitude in certain high peak load low duty cycle applications. Since the adding of PCM increases the thermal capacitance of the heat sink while also increasing its thermal resistance, care must be taken when selecting a heat sink configuration: the adding of PCM lowers the temperature only over a certain range of operation. Once the PCM has completely melted, the temperature eventually increases over that of a conventional heat sink. Furthermore, the utilization of the advantages of the PCM for each pulse requires complete re-solidification during the off-time. Therefore, the right configuration is strongly dependent on the application: the power pulse amplitude, period, and duty cycle.

In this paper, previous work on heat sink optimization was extended to create a thermal network model of a hybrid PCM heat sink. This allows for quick simulations of different heat sink configurations, so that an optimum design can be chosen. The optimization procedure presented in this paper is a good guide in selecting an optimum set of heat sink dimensions.

Looking at Figs. 8 and 9, a conclusion can be also drawn about the general usefulness of the organic PCM materials typically studied in literature and examined in this paper: they do not melt quickly enough to be of benefit in situations where the pulses are only several seconds or shorter. The use of PCM materials their use confer the most benefit in applications where the power pulse width is several minutes long and the period is measured in tens of minutes. In such applications, the peak temperature can be reduced by 10-20°C, which is an improvement. The use of PCM-metal foam can potentially make PCM hybrid heat sinks useful in applications where the pulse is several seconds or tens of seconds long.

8 Literature

[1] T. Wijekoon, L. Empringham, P. Wheeler, J. Clare, ‘‘Compact Dual-output Power Converter for an Aerospace Electrical Landing Gear Actuation System,’’ *Proc. EPE 2009,* Barcelona, September 2009.

[2] SINAUTEC Ultracap Bus factsheet, available at http://www.sinautecus.com/products.html

[3] M. Ciappa, F. Carhognani, P. Cow, W. Fichtner, “Lifetime Prediction and Design of Reliability Tests for High-Power Devices in Automotive Applications”, *IEEE Transactions on Device and Materials Reliability*, Vol.3, No.4, December 2003.

[4] M. Ciappa, “Lifetime Prediction on the Base of Mission Profiles”, *Microelectronics Reliability 45*, pp. 1293-1298, 2005.

[5] J. Leland, G. Recktenwald, “Optimization of a Phase Change Heat Sink for Extreme Environments," *19th IEEE semi-term symposium*, 2003.

[6] S. Krishnan, S. V. Garimella, S. S. Kang, “A Novel Hybrid Heat Sink using Phase Change Materials for Transient Thermal Management of Electronics," *IEEE Transactions on Components and Packaging Technologies*, Vol. 28, No. 2, June 2005.

[7] S. Krishnan, S. V. Garimella, “Analysis of a Phase Change Energy Storage System for Pulsed Power Dissipation,“ *IEEE Transactions on Components and Packaging Technologies*, Vol. 27, No. 1, March 2004.

[8] B. Liu, P. Majumdar, “Numerical Simulation of Phase Change Heat Transfer in PCM-encapsulated Heat Sinks," *18th IEEE semi-term symposium*, 2002.

[9] E. M. Alawadhi, C. Amon, “PCM Thermal Control Unit for Portable Electronic Devices: Experimental and Numerical Studies,” *IEEE Transactions on Components and Packaging Technologies*, Vol. 26, No. 1, March 2003.

[10] U. Drofenik, G. Laimer, J. W. Kolar, “Theoretical Converter Power Density Barriers for Forced Convection Cooling,“ *Proc. PCIM Europe 2005*, Nuremberg, June 2005.

[11] U. Drofenik, J. W. Kolar, “Analyzing the Theoretical Limits of Forced Air-Cooling by Employing Advanced Composite Materials with Thermal Conductivities > 400W/mK,” *Proc. 4th International Conference on Integrated Power Systems (CIPS'06),* Naples, June 2006.

[12] U. Drofenik, G. Laimer, J. W. Kolar, "Pump Characteristic Based Optimization of a Direct Water Cooling System for a 10kW/500kHz Vienna Rectifier", *IEEE Transactions on Power Electronics*, vol. 20, no. 3, pp. 704-714, May 2005.

[13] N. Zheng, R. A. Wirtz, “A Hybrid Thermal Energy Storage Device, Part 1: Design Methodology,” *ASME Journal of Electronic Packaging*, Vol. 126, March 2004.

[14] L. Huang, M. Petermann, C. Doetsch, “Evaluation of Paraffin/Water Emulsion as a Phase Change Slurry for Cooling Applications,” *Energy 34*, pp. 1145-1155, 2009.

[15] P. A. Espinoza Vallejos, C. Duston, “Carbon Foam Filled with Phase Change Materials for Passive Temperature Management,” *Proc. COMSOL Multiphysics User’s Conference*, Boston, 2005.

[16] Dong-won Yoo and Yogendra K. Joshi, “Energy Efficient Thermal Management of Electronic Components

ISBN 978-3-8007-3212-8

Using Solid–Liquid Phase Change Materials," *IEEE Transactions on Device and Materials Reliability*, Vol. 4, No. 4, December 2004.

[17] V. Shanmugasundaram, J. R. Brown, K. L. Yerkes, "Thermal Management of High Heat Flux Sources using Phase Change Material: A Design Optimization Procedure", *Proc. 32nd AIAA Thermophysics Conference*, Atlanta, June 1997.

[18] V.S.S. Srinivas, G.K. Ananthasuresh, "Analysis and Topology Optimization of Heat Sinks with a Phase-Change Material on COMSOL Multiphysics™ Platform," *Proc. COMSOL Multiphysics User's Conference*, Bangalore, 2006.

[19] Sanyo Denki fans, http://www.sanyodenki.eu/

ISBN 978-3-8007-3212-8